Modeling and Simulation of a Step-up Resonant Converter for DC Motor Drive

Ch.Manoj[1], Kolli Nageswar Rao[2]
[1] M.Tech Scholar, Department of Electrical & Electrical Engineering, Sree Vahini Institute of Science and Technology, Tiruvuru
[2] Assistant Professor, Department of Electrical & Electrical Engineering, Sree Vahini Institute of Science and Technology, Tiruvuru

Abstract : In this paper introduce a Step up Resonant Converter for DC Motor Drive. DC motors form the backbone of many industries and as such their speed control becomes of immense importance. It is a promising option to connect the renewable energy sources to the HVDC grid with a pure dc system and DC motor drive, in which high-power high-voltage step-up dc–dc converters are the key equipment to transmit the electrical energy. The converter can achieve high voltage gain using an LC parallel resonant tank. It is characterized by zero-voltage-switching (ZVS) turn-on and nearly ZVS turn-off of main switches as well as zero-current-switching turn-off of rectifier diodes; moreover, the equivalent voltage stress of the semiconductor devices is lower than other resonant step-up converters. The operation principle of the converter and its resonant parameter selection is presented in this project. Finally, the proposed converter simulated when connected to HVDC grid and DC motor drive conditions in MATLAB/SIMULINK and results verified.

Keywords – DC Motor Drive, Renewable energy, resonant converter, soft switching, voltage step-up, voltage stress

I. INTRODUCTION

Renewable energy production has been steadily increasing as international goals to reduce dependence on fossil fuels have been on the agenda for nations worldwide. Solar photovoltaic (PV) power systems are becoming a prevalent renewable energy option with the cost of PV cells decreasing and their solar conversion efficiency increasing [1]-[2]. DC motors form the backbone of many industries and as such their speed control becomes of immense importance. It has been found that many of these applications perform with a greater efficiency when the motors are fed from a source of variable dc power. The good speed control methods available in DC motor drives even low ratings and high ratings. A high rating DC motor drives has the application in Submarines [2]-[6]. Generally solar and wind powers are complementary in nature. Therefore the hybrid photovoltaic and wind energy system has higher dependability to give steady power than each of them operating individually. Other benefit of the hybrid system is that the amount of the battery storage can be decreased as hybrid system is more reliable compared to their independent operation. At present, the voltages over the dc stages in the generation equipments of the renewable energy sources are relatively low, in the range of several hundred volts to several thousand volts; hence, high-power high-voltage step-up dc–dc converters are required to deliver the produced electrical energy to the HVDC grid. Furthermore, as the connectors between the renewable energy sources and HVDC grid, the step-up dc–dc converters not only transmit electrical energy, but also isolate or buff kinds of fault conditions; they are one of the key equipments in the dc grid [7].

Recently, the high-power high-voltage step-up dc–dc converters have been studied extensively. The transformer is a convenient approach to realize voltage step-up. The classic full-bridge (FB) converter, single active bridge (SAB) converter, and LCC resonant converter are studied and their performance is compared for the offshore wind farm application. The three-phase topologies, such as three-phase SAB converter, series resonant converter, and dual active bridge converter, which are more suitable for high-power applications due to alleviated current stress of each bridge, are also studied and designed for high-power high-voltage step-up applications. The emerging modular dc–dc converter, which uses two modular multilevel converters linked by a medium-frequency transformer, is well suited for the application in the HVDC grid [8].

The soft-switching technology is critical to improve the conversion efficiency, especially for high-voltage applications. Recently, several soft-switching topologies for high-power high-voltage applications have been proposed. In [9] and [10], the converter topologies based on resonant switched capacitor (RSC) are proposed with reduced switching loss and modular structure. The shortage of the RSC-based converter is the poor voltage regulation and the requirement of a large number of capacitors. Jovcic et al. proposed a novel type of resonant step-up converter with potentially soft-switching operation, which utilizes thyristors as switches and does not suffer from excessive switch stresses and reverse recovery problems; moreover, a large voltage gain is easily obtained. Similarly, in [11], a new family of resonant transformer-less modular dc-dc converters is proposed and the main feature of the proposed converters is that the unequal voltage stress on semiconductors of thyristor valve is avoided with the use of active switching net- work, which is composed of an ac capacitor and four identical active switches. Thyristors have large voltage and current ratings; however, the use of thyristor limits the switching frequency of the converter, resulting in bulky passive components and slow dynamic response [30]. Moreover, the resonant inductors of the converters are unidirectional magnetized in [12], leading to lower utilization of the magnetic core, which means that a great volume of core is required. In this paper, a novel resonant step-up dc–dc converter is proposed, which not only can realize soft switching for main switches and diodes and large voltage gain, but also has relatively lower equivalent voltage stress of the semiconductor devices and bidirectional magnetized resonant inductor.

The operation principle of the converter and the design of the resonant parameters are presented in this project. This High voltage converter studied under the DC motor Drive by MATLAB/SIMULINK.

II. CONVERTER STRUCTURE AND OPERATION PRINCIPLE

The proposed resonant step-up converter is shown in Fig. 1 The converter is composed of an FB switch network, which comprises Q1 through Q4, an LC parallel resonant tank, a voltage doubler rectifier, and two input blocking diodes, Db1 and Db2. The steady-state operating waveforms are shown in Fig. 2 and detailed operation modes of the proposed converter are shown in Fig. 3. For the proposed converter, Q2 and Q3 are tuned on and off simultaneously; Q1 and Q4 are tuned on and off simultaneously. In order to simplify the analysis of the converter, the following assumptions are made:

1) all switches, diodes, inductor, and capacitor are ideal components;

2) output filter capacitors C1 and C2 are equal and large enough so that the output voltage Vo is considered constant in a switching period Ts.

A. Mode 1 [t0, t1] [See Fig. 3(a)]

During this mode, Q1 and Q4 are turned on resulting in the positive input voltage Vin across the LC parallel resonant tank, i.e., vLr = vC r = Vin. The converter operates similar to a conventional boost converter and the resonant inductor Lr acts as the boost inductor with the current through it increasing linearly from I0. The load is powered by C1 and C2. At t1, the resonant inductor current iLr reaches I1.

$$I_1 = I_0 + \frac{V_{\text{in}} T_1}{L_r} \qquad (1)$$

Where T1 is the time interval of t0 to t1.

Fig. 1. Topology of the proposed resonant step-up converter

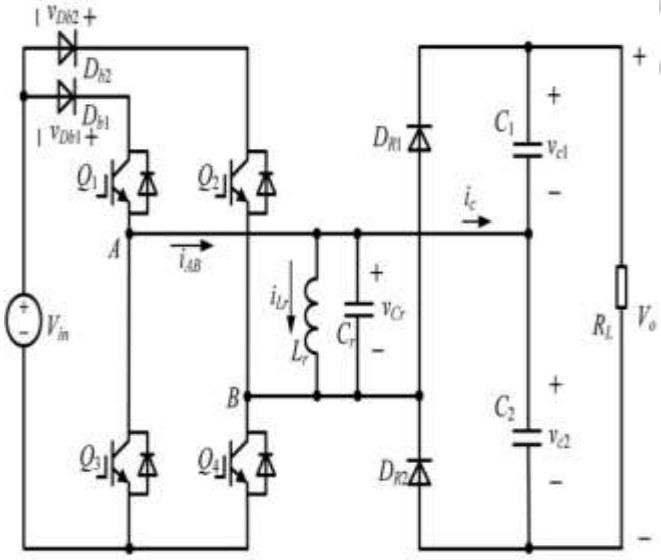

Fig. 2. Operating waveforms of the proposed converter

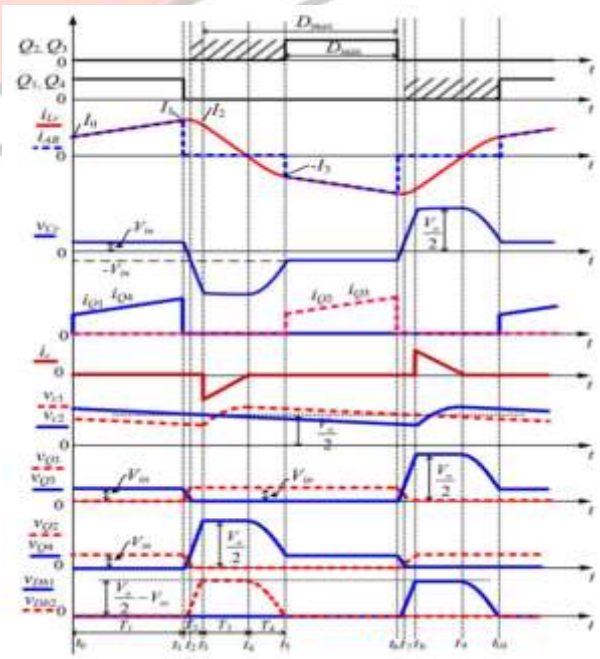

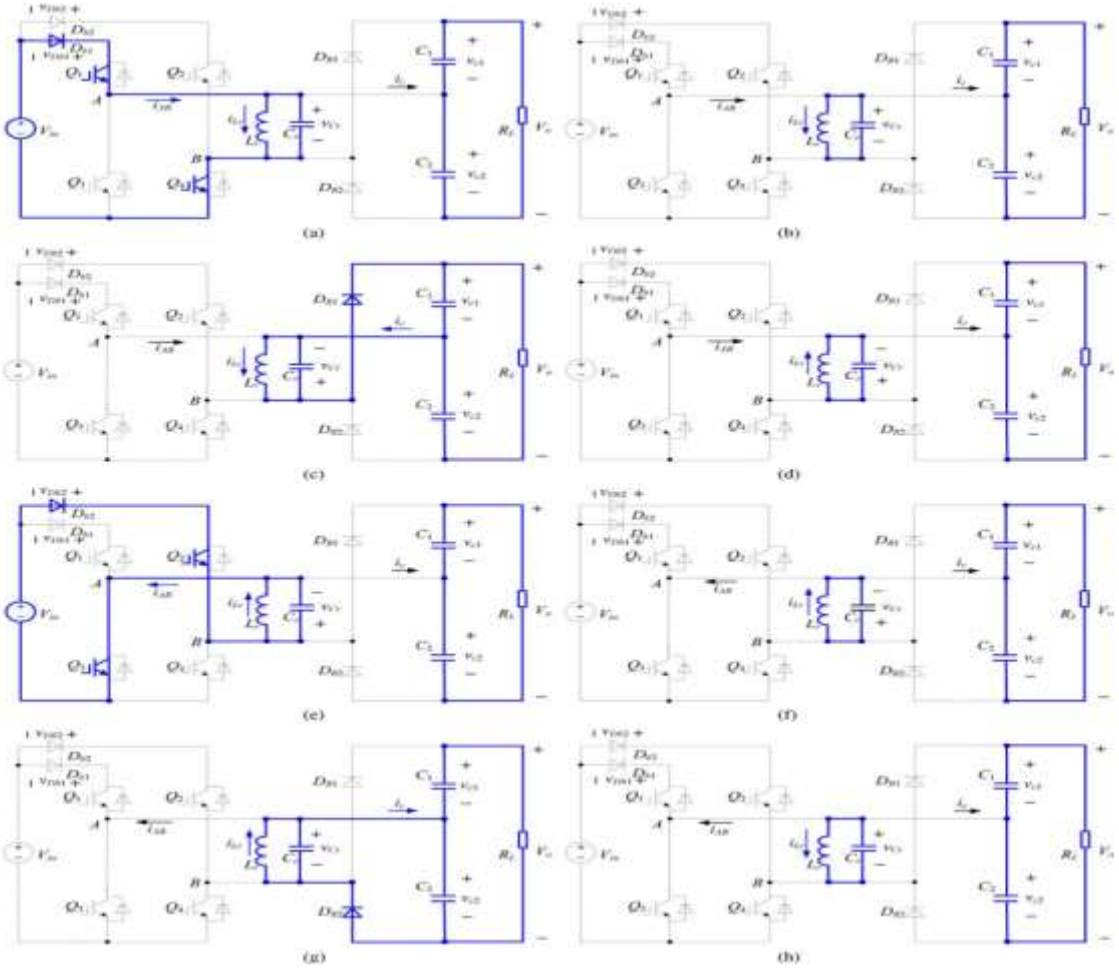

Fig. 3. Equivalent circuits of each operation stages. (a) [t0 , t1]. (b) [t1 , t3]. (c) [t3 , t4]. (d) [t4 , t5]. (e) [t5 , t6]. (f) [t6 , t8]. (g) [t8 , t9]. (h) [t9 , t10].

In this mode, the energy delivered from Vin to Lr is

$$E_{\text{in}} = \frac{1}{2} L_r (I_1^2 - I_0^2) \tag{2}$$

B. Mode 2 [t1, t3] [See Fig. 3(b)]

At t1, Q1 and Q4 are turned off and after that Lr resonates with Cr, vC r decreases from Vin, and iLr increases from I1 in resonant form. Taking into account the parasitic output Capacitors of Q1 through Q4 and junction capacitor of Db2, the equivalent circuit of the converter after t1 is shown in Fig. 4(a), in which CDb2, CQ1, and CQ4 are charged, CQ2 and CQ3 are discharged. In order to realize zero-voltage switching (ZVS) for Q2 and Q3, an additional capacitor, whose magnitude is about ten times with respect to CQ2, is connected in parallel with Db2. Hence, the voltage across Db2 is considered unchanged during the charging/discharging process and Db2 is equivalent to be shorted. Due to Cr is much larger than the parasitic capacitances, the voltages across Q1 and Q4 increase slowly.

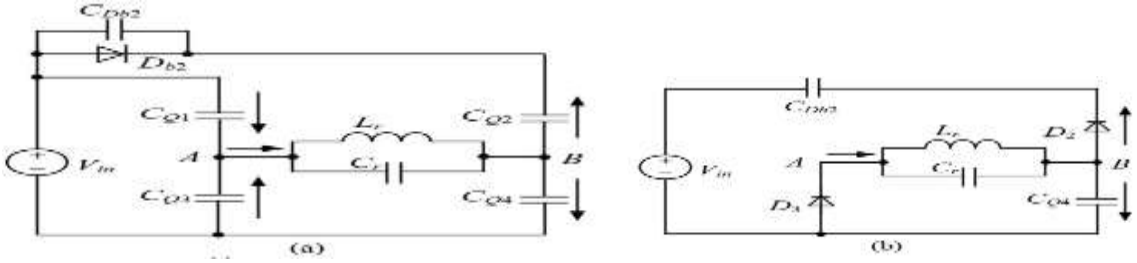

Fig. 4. Further equivalent circuits of Mode 2. (a) [t1 , t2]. (b) [t2 , t3].

As a result, Q1 and Q4 are turned off at almost zero voltage in this mode. When vCr drops to zero, iLr reaches its maximum magnitude. After that, vC r increases in negative direction and iLr declines in resonant form. At t2, vCr = −Vin, the voltages across Q1 andQ4 reach Vin, the voltages across Q2 and Q3 fall to zero and the two switches can be turned on under zero-voltage condition.

It should be noted that although Q2 and Q3 could be turned on after t2, there are no currents flowing through them. Aftert2, Lr continues to resonate with Cr, vCr increases in negative direction from −Vin, iLr declines in resonant form. Db2 will hold reversed-bias voltage and the voltage across Q4 continue to increase from Vin. The voltage across Q1 is kept at Vin. The equivalent circuit of the converter after t2 is shown in Fig. 4(b), in which D2 and D3 are the anti-parallel diodes of Q2 and Q3, respectively. This mode runs until vCr increases to −Vo/2 and iLr reduces to I2, at t3, the voltage across Q4 reaches Vo/2 and the voltage across Db2 reaches Vo/2 − Vin. It can be seen that during t1 to t3, no power is transferred from the input source or to the load, and the whole energy stored in the LC resonant tank is unchanged, i.e.,

$$\frac{1}{2}L_r I_1^2 + \frac{1}{2}C_r V_{\text{in}}^2 = \frac{1}{2}L_r I_2^2 + \frac{1}{2}C_r \left(\frac{V_o}{2}\right)^2 \tag{3}$$

$$i_{Lr}(t) = \frac{V_{\text{in}}}{Z_r}\sin\left[\omega_r(t-t_1)\right] + I_1\cos\left[\omega_r(t-t_1)\right] \tag{4}$$

$$v_{Cr}(t) = V_{\text{in}}\cos\left[\omega_r(t-t_1)\right] - I_1 Z_r \sin\left[\omega_r(t-t_1)\right] \tag{5}$$

$$T_2 = \frac{1}{\omega_r}\left[\arcsin\left(\frac{V_{\text{in}}}{\sqrt{V_{\text{in}}^2 + \frac{L_r I_1^2}{C_r}}}\right) + \arcsin\left(\frac{V_o}{2\sqrt{V_{\text{in}}^2 + \frac{L_r I_1^2}{C_r}}}\right)\right] \tag{6}$$

Where ωr = 1√LrCr, Zr = Lr/Cr, and T2 is the time interval of t1 to t3.

C. Mode 3 [t3, t4] [See Fig.3(c)]

At t3, vC r = −Vo/2, DR1 conducts naturally, C1 is charged by iLr through DR1, vC r keeps unchanged, and iLr decreases linearly. At t4, iLr = 0. The time interval of t3 to t4 is

$$T_3 = \frac{2I_2 L_r}{V_o} \tag{7}$$

The energy delivered to load side in this mode is

$$E_{\text{out}} = \frac{V_o I_2 T_3}{4} \tag{8}$$

The energy consumed by the load in half-switching period is

$$E_R = \frac{V_o I_o T_s}{2} \tag{9}$$

Assuming 100% conversion efficiency of the converter and according to the energy conversation rule, in half-switching period

$$E_{\text{in}} = E_{\text{out}} = E_{\text{R}} \tag{10}$$

Combining (7), (8), (9), and (10), we have

$$I_2 = V_o\sqrt{\frac{I_o T_s}{V_o L_r}} \tag{11}$$

$$T_3 = 2\sqrt{\frac{T_s I_o L_r}{V_o}} \tag{12}$$

D. Mode 4 [t4, t5] [See Fig. 3(d)]

At t4, iLr decreases to zero and the current flowing throughDR1 also decreases to zero, and DR1 is turned off with zero current switching (ZCS); therefore, there is no reverse recovery. After t4, Lr resonates with Cr, Cr is discharged through Lr, vCr increases from −Vo/2 in positive direction, and iLr increases from zero in negative direction. Meanwhile, the voltage acrossQ4 declines from Vo/2. At t5, vC r = −Vin, and iLr = −I3. In this mode, the whole energy stored in the LC resonant tank is unchanged, i.e., where T4 is the time interval of t4 to t5.

$$\frac{1}{2}C_r\left(\frac{V_o}{2}\right)^2 = \frac{1}{2}L_r I_3^2 + \frac{1}{2}C_r V_{\text{in}}^2 \quad (13)$$

$$I_0 = I_3 = \frac{1}{2}\sqrt{\frac{C_r(V_o^2 - 4V_{\text{in}}^2)}{L_r}} \quad (14)$$

$$i_{Lr}(t) = -\frac{V_o}{2\omega_r L_r}\sin\left[\omega_r(t - t_5)\right] \quad (15)$$

$$v_{Cr}(t) = \frac{-V_o\cos\left[\omega_r(t - t_5)\right]}{2} \quad (16)$$

$$T_4 = \frac{1}{\omega_r}\text{arc}\cos\left(\frac{2V_{\text{in}}}{V_o}\right) \quad (17)$$

E. Mode 5 [t5, t6] [See Fig. 3(e)]

If Q2 and Q3 are turned on before t5, then after t5, Lr is charged by Vin through Q2 and Q3, iLr increases in negative direction, and the mode is similar to Mode 1.If Q2 and Q3 are not turned on before t5, then after t5, Lr will resonate with Cr, the voltage of node A vA will increase from zero and the voltage of node B vB will decay from Vin; zero-voltage condition will be lost if Q2 and Q3 are turned on at the moment. Therefore, Q2 and Q3 must be turned on beforet5 to reduce switching loss. The operation modes during [t6, t10] are similar to Modes2–4, and the detailed equivalent circuits are shown in Fig. 3(f)–(h). During [t6, t10], Q2 and Q3 are turned off at almost zero voltage, Q1 and Q4 are turned on with ZVS, and DR2 is turned off with ZCS.

III. DC MOTOR DRIVE

The speed of a DC Motor is directly proportional to the line voltage applied to it. Given a fixed DC source, V_S, and a Power GTO to act as a switch, it is possible to control the average voltage applied to the motor using a technique called Pulse-Width Modulation (PWM). The source voltage, Vs, is "chopped" to produce an average voltage somewhere between 0% and 100% of Vs. Thus the average value of the voltage applied to the Motor, Vm, is controlled by closing and opening the "switch", Q1. To close the switch, a firing signal is delivered to the gate of the GTO, causing it to conduct between source and drain. To open the switch, the firing signal is removed and the GTO is self-biased to stop conducting. In PWM, the switch is closed and opened every modulation period. The voltage, Vm, seen by the motor can be expressed in terms of the source voltage, Vs, and the "ON" time, t_1, and the period of modulation, T. The equation is:

$$Vm = \alpha\, Vs \qquad \text{where } \alpha = t_1 / T$$

The symbol α is called the Duty Cycle. As duty cycle is increased from 0% to 100%, the average voltage applied to the motor increases from 0 to Vs volts and the motor speeds up.

Table 1 Simulation Parameters

Parameter	Value
Input voltage	4 KV
Output voltage	58 KV
Resonant inductance	600 μH
Resonant capacitance	1.68 μF
Filter capacitance	22 μF

IV. MATLAB/SIMULATION RESULTS

In order to verify the operation principle and the theoretical analysis, a converter is simulated with MATLAB/SIMULINK simulation software and the detailed parameters are listed in Table 5. Figure 5 shows a SIMULINK model of 5 MW load of proposed concept converter.

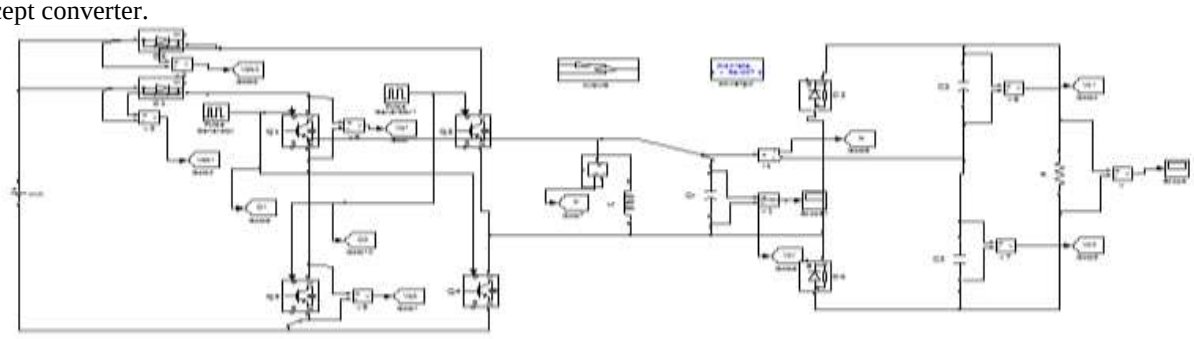

Figure 5: SIMULINK block diagram under 5MW load condition

Figure 6: Simulation waveform of the switching pulses (Q1, Q2, Q3 and Q4) for 5MW

Figure 6 to 10 shows the simulation results at the output power of 5MW (Vin = 4 kV), respectively. As the figure shows, the voltage stress of Q1 and Q2 is 4 kV, the voltage stress of Q3 and Q4 is 40 kV, the voltage stress of Db1 and Db2 is 36 kV, and the peak voltage across the LC resonant tank is 40 kV.

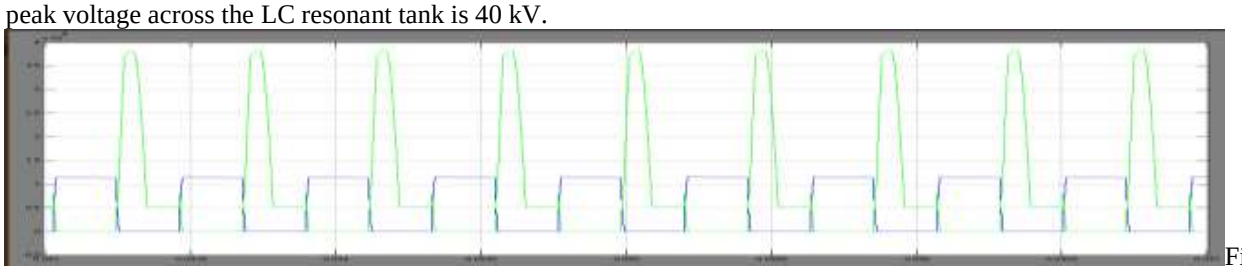

Figure 7: Simulation waveform of the switch voltages (VQ1 and VQ2) for 5MW

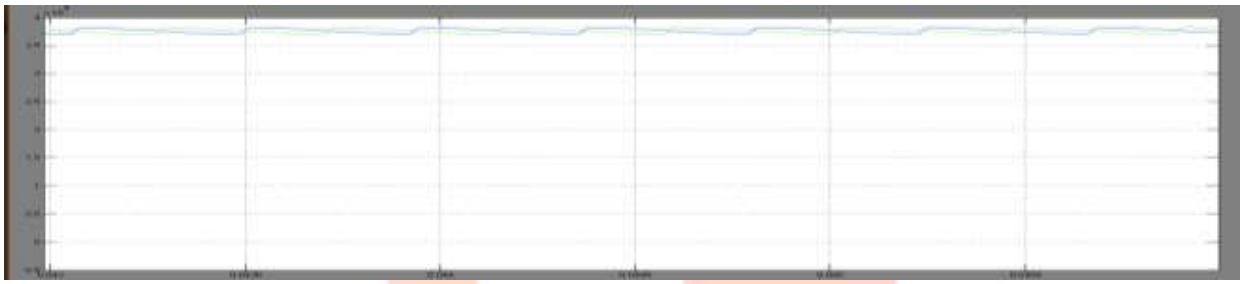

Figure 8: Simulation waveform of the output filter Capacitor Voltages (VC1 and VC2)

Q1 through Q4 are turned on under zero-voltage condition and when they are turned off, the voltage across the device increases slowly from zero. The switching frequencies of the converter at 5 and 1 MW are 2.3 and 4.4 kHz, respectively. The simulation results match well with the aforementioned analysis

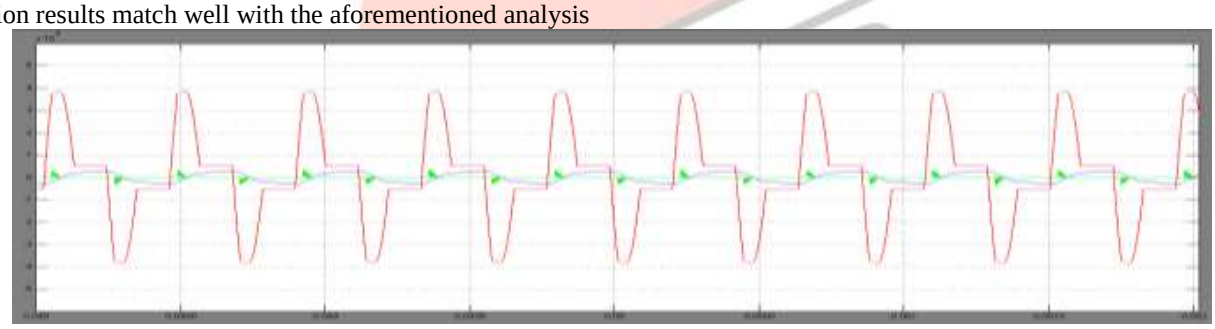

Figure 9: simulation waveform of resonant inductor current iLr, capacitor voltage and capacitor Current for 5MW

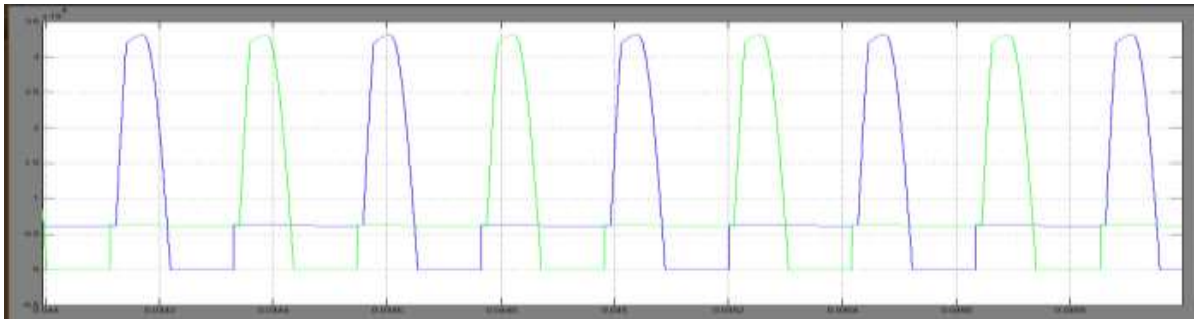

Figure 10: Simulation waveform of the input blocking diodes Voltages (VDb1 and VDb2) for 5MW

Figure 11 to 15 shows the simulation results at the output power of 1 MW (Vin = 4 kV), respectively. The switching frequencies of the converter at 5 and 1 MW are 2.3 and 4.4 kHz, respectively. The simulation results match well with the aforementioned analysis.

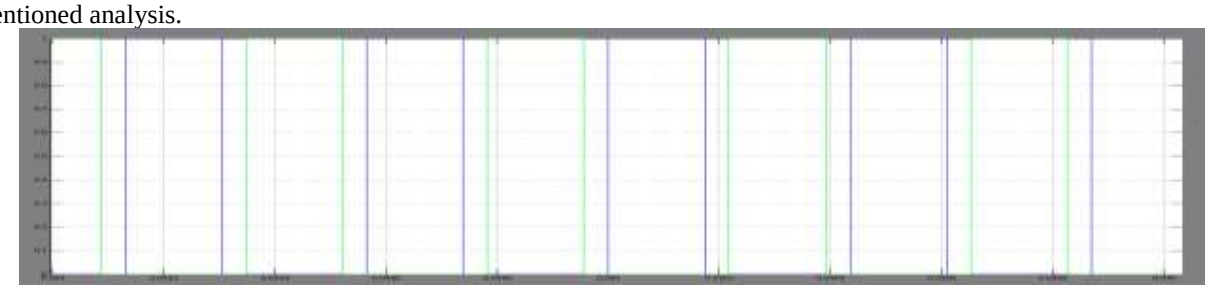

Figure 11: Simulation waveform of the switching pulses (Q1, Q2, Q3 and Q4) for 1MW.

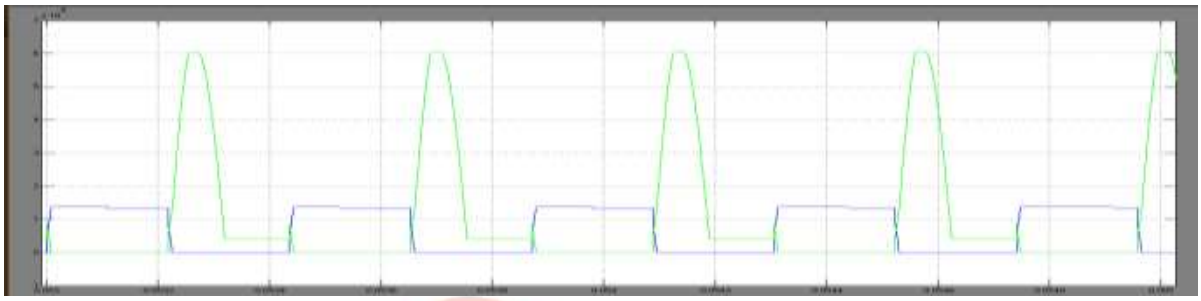

Figure 12: Simulation waveform of the switch voltages (VQ1 and VQ2) for 1MW

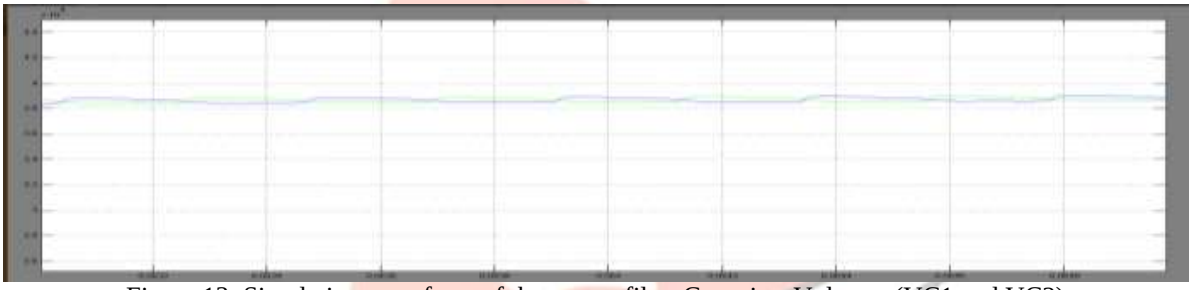

Figure 13: Simulation waveform of the output filter Capacitor Voltages (VC1 and VC2)

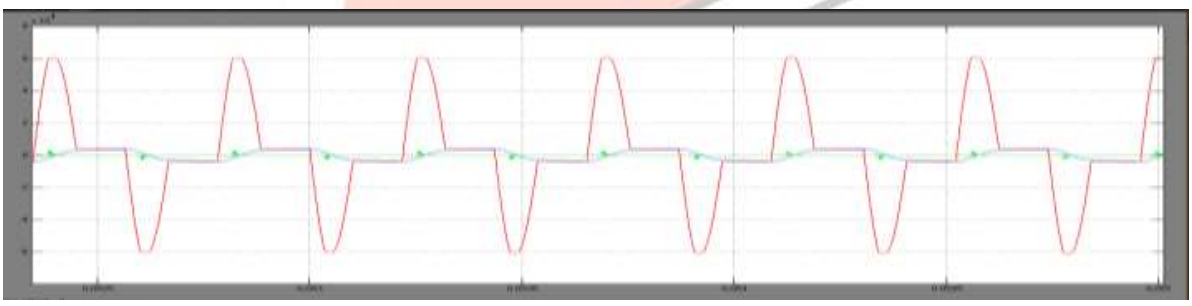

Figure 14: simulation waveform of resonant inductor current iLr, capacitor voltage and capacitor Current for 1MW

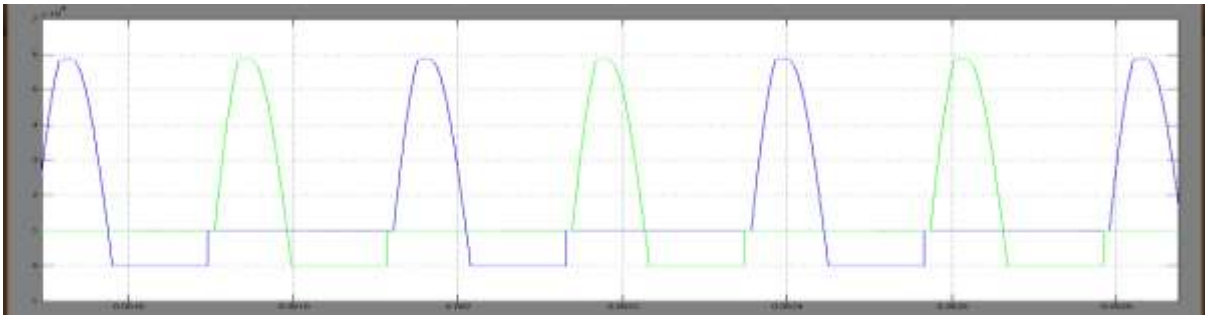

Figure 15: Simulation waveform of the input blocking diodes Voltages (VDb1 and VDb2) for 1MW

Figure 16 shows the SIMULINK block diagram of Input voltage step (Dynamic Simulation condition). The simulation results corresponding to a step change of input voltage from 4 to 4.4 kV under full-load condition. It can be seen that the output voltage is regulated to be constant and the switching frequency fs changes from 2.3 to 2.5 kHz.

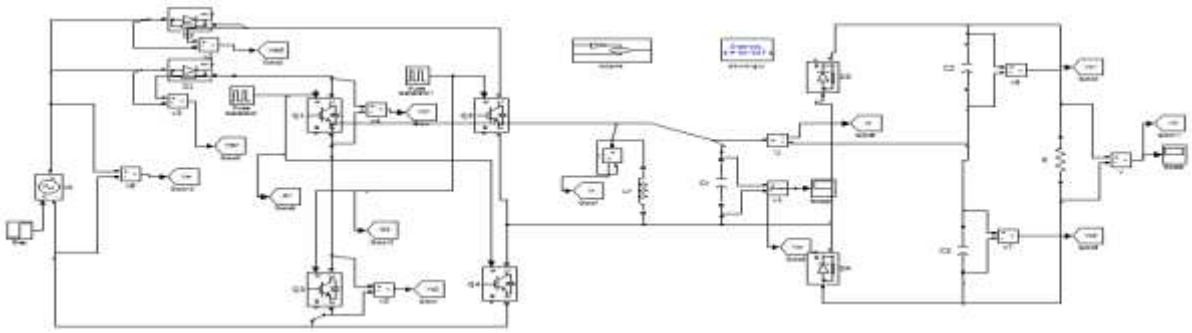

Figure 16: Simulink block diagram for input voltage step (Dynamic)

Figure 17 to 19 illustrates the simulation results corresponding to a load stepping from full load to 40% load under 4 kV input voltage condition. It can be seen that the output voltage is regulated to be constant and the switching frequency fs changes from 2.3 to 3.8 kHz.

Figure 17: Step Input Voltage

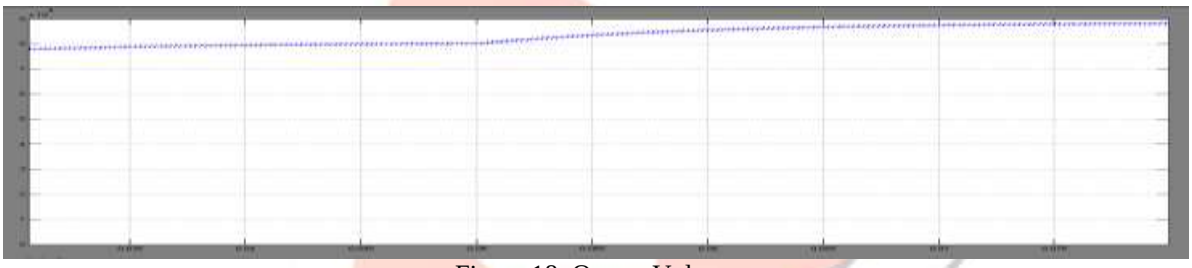

Figure 18: Output Voltage

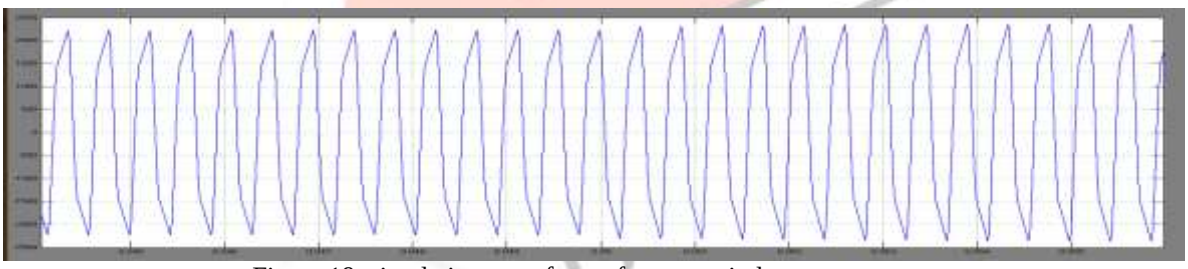

Figure 19: simulation waveform of resonant inductor current iLr

Figure 20 shows the SIMULINK model diagram of a step up resonant converter fed DC motor drive. The simulation results corresponding to a step up resonant converter fed DC motor drive. It can be seen that the output voltage is regulated to be constant and the switching frequency fs changes from 2.3 to 2.5 kHz.

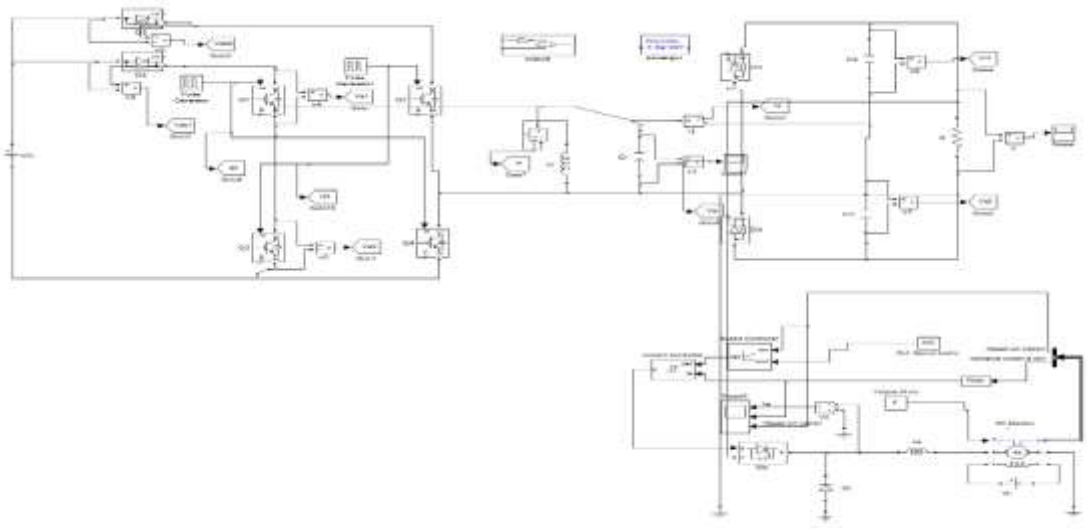

Figure 20: Simulink block diagram of Step-up Resonant Converter fed DC Motor drive

Now a day's High rating DC motors are used in submarine applications. This High rating DC Motor drive connected across the high voltage of proposed step up resonant converter as shown in figure 20. GTO switch is used because of high switching frequency and high rating. This DC motor drive is closed loop operation depends on reference speed (rad/sec). Speed controller consists of PI controller (p = 0.1 and K_I = 0.01). Hysteresis controller used as a current limiter (current control, current limit is 1A). The purpose of filter in the closed circuit is to reduce the ripple in the armature current for the best control.

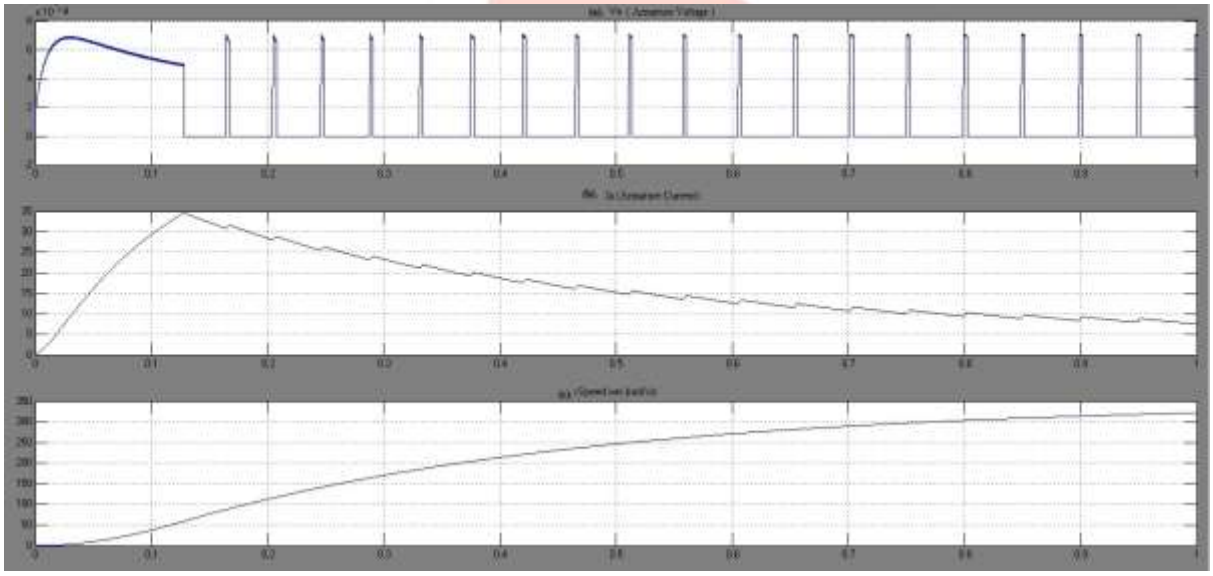

Figure 21: Simulation results of DC motor drive (a). Armature Voltage, (b). Armature Current, (c) Speed in rad/sec

Figure 21 (a), (b) and (c), shows the output results of DC motor drive under the proposed step up resonant converter. Here we presented the separately excited DC motor. The armature voltage is pulsating voltage because of closed loop controller the control switch (GTO) ON/OFF by the switching angle generated by current control as shown in simulink model diagram figure 20. Figure 21 (a) the voltage of armature has high, it is clear that the proposed working perfect even it high rating DC Motor drive.

DC machine speed also maintains the reference speed (330 rad/sec) as shows in the figure 21 (c). The armature current also works well from figure 21. From the above results the DC motor drive works very perfectly under the proposed a step up resonant converter.

V. CONCLUSION

The good speed control methods available in DC motor drives even low ratings and high ratings. A high rating DC motor drives has the application in Submarines. A novel resonant dc–dc converter is proposed in this project, which can achieve very high step-up voltage gain and it is suitable for high-power high-voltage applications. The resonant capacitor is employed to achieve zero-voltage turn-on and turn-off for the active switches and ZCS for the rectifier diodes. The analysis demonstrates that the converter can operate at any gain value (>2) with proper control; however, the parameters of the resonant tank determine the maximum switching frequency, the range of switching frequency, and current ratings of active switches and diodes. The converter is controlled by the variable switching frequency. Simulation results verify the operation principle of the converter under the pure resistor, variable input voltage and DC motor drive. DC motor drive performed well operation from results. Therefore this converter very use full to high voltage high power applications.

REFERENCES

[1] S. Abdel-Khalik, A. M. Massoud, A. A. Elserougi, and S. Ahmed, "Optimum power transmission-based droop control design for multi-terminal HVDC of offshore wind farms," IEEE Trans. Power Syst., vol. 28, no. 3, pp. 3401–3409, Aug. 2013.

[2] F. Deng and Z. Chen, "Design of protective inductors for HVDC transmission line within DC grid offshore wind farms," IEEE Trans. Power Del., vol. 28, no. 1, pp. 75–83, Jan. 2013.

[3] F. Deng and Z. Chen, "Operation and control of a DC-grid offshore wind farm under DC transmission system faults," IEEE Trans. Power Del., vol. 28, no. 1, pp. 1320–1363, Jul. 2013.

[4] Zuo Z. Liu,Frang L. Luo, Rashid M.H., High performance nonlinear MIMO field weakening controller of a separately excited dc motor, Electric Power System research, Vol 19, Issue 3, 2000, pp(121-164)

[5] W. Chen, A. Huang, S. Lukic, J. Svensson, J. Li, and Z. Wang, "A comparison of medium voltage high power DC/DC converters with high step-up conversion ratio for offshore wind energy systems," in Proc. IEEE Energy Convers. Congr. Expo., 2011, pp. 584–589.

[6] S. Fan, W. Ma, T. C. Lim, and B. W. Williams, "Design and control of a wind energy conversion system based on a resonant dc/dc converter," IET Renew. Power Gener., vol. 7, no. 3, pp. 265–274, 2013.

[7] C. Meyer, M. Hoing, A. Peterson, and R. W. De Doncker, "Control and ¨ design of DC grids for offshore wind farms," IEEE Trans. Ind. Appl., vol. 43, no. 6, pp. 1475–1482, Nov./Dec. 2007.

[8] T. Luth, M. Merlin, T. Green, F. Hassan, and C. Barker, "High frequency operation of a DC/AC/DC system for HVDC applications," IEEE Trans. Power Electron., vol. 29, no. 8, pp. 4107–4115, Aug. 2014.

[9] C. Meyer and R. W. De Doncker, "Design of a three-phase series resonant converter for offshore DC grids," in Proc. IEEE Ind. Appl. Soc. Conf., 2007, pp. 216–223.

[10] C. Meyer, M. Hoing, A. Peterson, and R. W. De Doncker, "Control and ¨ design of DC grids for offshore wind farms," IEEE Trans. Ind. Appl., vol. 43, no. 6, pp. 1475–1482, Nov./Dec. 2007.

[11] Mohan, Ned, Power Electronics, John Wiley and Sons, 1989

[12] MATLAB SIMULINK, version 2009, SimPowerSystem, One quadrant chopper DC drive.